

Hypochlorous Acid Promoted Platinum Drug Chemotherapy by Myeloperoxidase-Encapsulated Therapeutic Metal Phenolic Nanoparticles

Yunlu Dai,^{†,‡} Siyuan Cheng,[‡] Zhongliang Wang,^{*,†} Ruili Zhang,[†] Zhen Yang,[‡] Jingjing Wang,[‡] Bryant C. Yung,[‡] Zhantong Wang,[‡] Orit Jacobson,[‡] Can Xu,[‡] Qianqian Ni,[‡] Guocan Yu,[‡] Zijian Zhou,[‡] and Xiaoyuan Chen^{*,‡}

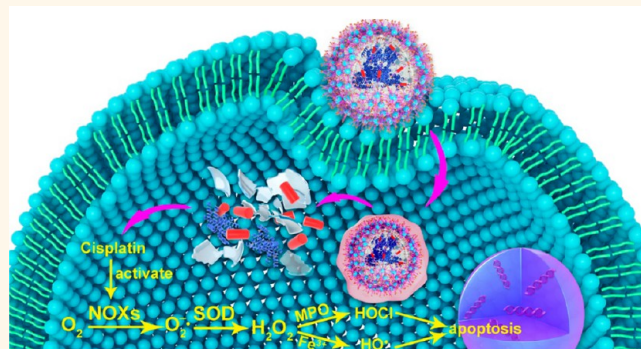
[†]Engineering Research Center of Molecular-imaging and Neuro-imaging of Ministry of Education, School of Life Science and Technology, Xidian University, Xi'an, Shaanxi 710126, China

[‡]Laboratory of Molecular Imaging and Nanomedicine (LOMIN), National Institute of Biomedical Imaging and Bioengineering (NIBIB), National Institutes of Health (NIH), Bethesda, Maryland 20892, United States

Supporting Information

ABSTRACT: This study applies *in situ* production of hypochlorous acid (HOCl) to improve the therapeutic efficacy of platinum drugs. The phagocytic enzyme myeloperoxidase (MPO) is coated with two functional polyphenol derivatives (platinum prodrug polyphenols and PEG polyphenols) and ferric ion by metal phenolic coordination, which can shield MPO from degradation by other compounds in the blood. Moreover, the platinum prodrug can be reduced to cisplatin in cells and produce hydrogen peroxide (H₂O₂). The MPO catalyzes the conversion of H₂O₂ to HOCl in the intercellular environment. The as-prepared MPO Pt PEG nanoparticles (MPP NPs) can be employed as a reactive oxygen species cascade bioreaction to enhance platinum drug therapy. The MPP NPs show prolonged blood circulation and high tumor accumulation as evidenced by ⁸⁹Zr-based positron emission tomography imaging. The MPP NPs effectively inhibit tumor growth *in vivo*. As a first-in-class platform to harness the highly toxic HOCl in nanomedicine for cancer therapy, this strategy may open doors for further development of progressive therapeutic systems.

KEYWORDS: myeloperoxidase (MPO), metal–polyphenol networks, hypochlorous acid (HOCl), cisplatin, positron emission tomography



Reactive oxygen species (ROS) are broadly defined as highly reactive chemical species, including hydroxyl radical (HO•), hydrogen peroxide (H₂O₂), superoxide radical (O₂^{•-}), and hypochlorite ion (OCl⁻).^{1,2} ROS play essential roles in cell signaling and regulation of cellular functions. There is a balance between the production and scavenging of ROS.³ Excessive ROS generation can disrupt cellular function and damage cell components.⁴ One of the promising therapeutic strategies to exploit ROS generation for cancer therapy is photodynamic therapy (PDT), which activates photosensitizing molecules by specific wavelengths of light to generate cytotoxic ROS to disrupt cellular function and promote cell death.^{5–10} However, the short penetration depth of light restricts its application for deep-seated tumors.¹¹ Additionally, the photosensitizing molecules have severe drawbacks, such as

poor water solubility, high toxicity to normal tissues, and poor specific delivery.¹² To address these issues, developing smart ROS generation platforms to improve the therapeutic efficiency is highly desired.

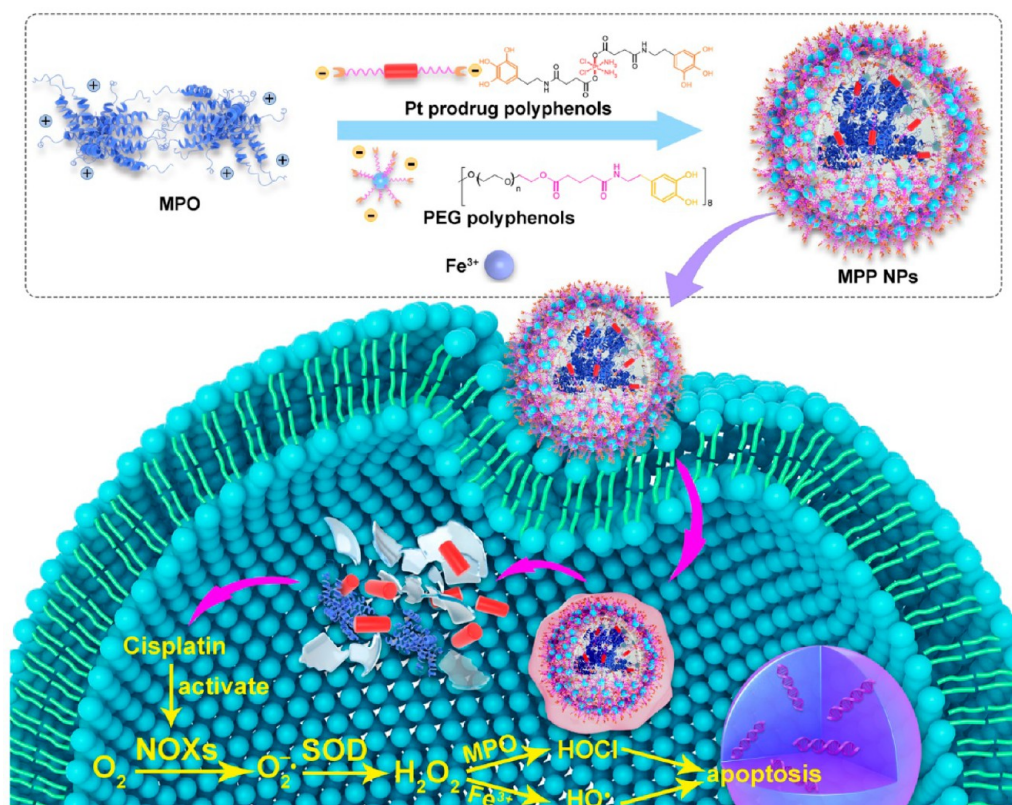
Nicotinamide adenine dinucleotide phosphate-oxidase (NOXs) is an important ROS-producing enzyme that donates electrons from NADPH inside the cell across the membrane and couples these to produce O₂^{•-}.^{13,14} As we know, the platinum-based anticancer drug cisplatin has been employed to treat a large quantity of cancers, such as ovarian cancer, brain cancer, and lung

Received: September 26, 2017

Accepted: December 31, 2017

Published: January 2, 2018

Scheme 1. Self-assembly of MPP NPs and the ROS generation process. The positively charged surface of MPO can adsorb negatively charged polyphenol derivatives by electrostatic interactions. The Fe^{3+} can be utilized to crosslink all the polyphenol derivatives together to form MPP NPs. In the intercellular environment, the Pt prodrug polyphenols were reduced to cisplatin, which activated NOXs. NOXs can catalyze O_2 to $\text{O}_2^{\bullet-}$, and SOD catalyzed H_2O_2 generation from $\text{O}_2^{\bullet-}$. MPO and ferric ions turned H_2O_2 into highly toxic HOCl and HO^\bullet , respectively.



cancer.^{15–17} Moreover, cisplatin can activate NOXs to produce $\text{O}_2^{\bullet-}$, which can be depleted to H_2O_2 by superoxide dismutases (SOD).¹⁸ H_2O_2 is converted downstream to highly toxic ROS, including OCl^- and HO^\bullet .^{19–21} The phagocytic enzyme myeloperoxidase (MPO) is a peroxidase enzyme expressed in neutrophil granulocytes.^{22,23} In the presence of the chloride ion, MPO can generate hypochlorous acid (HOCl) for antibacterial activity *via* the enzymatic reaction with H_2O_2 dismutated from $^1\text{O}_2$.²⁴ HOCl is a powerful ROS and can react with other molecules in the biological environment, such as proteins, DNA, and lipids by the oxidation process.²⁵ Thus, HOCl is an excellent candidate for tumor therapy applications.

Metal–polyphenol networks (MPNs), based on the coordination between the metal ion and phenolic ligands, have attracted wide attention because of several advantages including high biocompatibility, pH-responsive disassembly, and high mechanical stability.^{26,27} The MPNs not only can be used to construct nanomaterials with special morphologies but also have emerged as material surface modifiers.²⁸ To achieve a synergistic therapeutic platform for cancer treatment, we demonstrated that cisplatin prodrug can be integrated with ROS generation induced by MPO and metal ion for enhanced therapeutic efficiency. Two functional polyphenol derivatives with negative charge can adsorb onto the surface of MPO by electrostatic interactions. Then the Fe^{3+} can be utilized to cross-link all the polyphenol derivatives together to form MPP NPs (Scheme 1). Furthermore, the functional polyphenols derivatives create a physical barrier between MPO and the external environment to

protect the MPO from degradation and inactivation *in vivo*. The two functional polyphenol derivatives, platinum prodrug polyphenols and poly(ethylene glycol) (PEG) polyphenols, exhibit therapeutic ability and reduce nonspecific protein adsorption, respectively. Moreover, the platinum prodrug polyphenols can be reduced to yield cisplatin and further activate NOXs to elevate the $\text{O}_2^{\bullet-}$ level, which can be dismutated to H_2O_2 by SOD. Most importantly, the H_2O_2 can be converted to toxic HOCl by MPO catalysis. In addition, ferric ion can induce a Fenton reaction with H_2O_2 to generate HO^\bullet . Both HOCl and HO^\bullet would inflict serious damage to lipids in biomembranes. The integration of highly toxic ROS and a platinum drug developed a synergistic combination therapy. This strategy may establish a facile therapeutic approach for cancer treatment.

RESULTS AND DISCUSSION

Controlled Synthesis and Characterization of MPP NPs.

The platinum prodrug polyphenols were prepared by introducing two galloyl groups at the axial positions of cisplatin (as determined by ^1H NMR analysis, Figures S1 and S2).²⁸ PEG polyphenols were synthesized by conjugation of 8-arm-PEG-NHS (20 kDa) and dopamine.²⁹ This polymer was characterized by ^1H NMR spectroscopy (Figure S3). The MPO Pt PEG nanoparticles (MPP NPs) were fabricated by a one-step coating process. MPO was dissolved in phosphate-buffered saline (PBS). Platinum prodrug polyphenols, PEG polyphenols, and FeCl_3 were added into the above solution, and the pH was adjusted to 7.6 by Tris buffer to obtain MPP NPs. Energy-dispersive X-ray

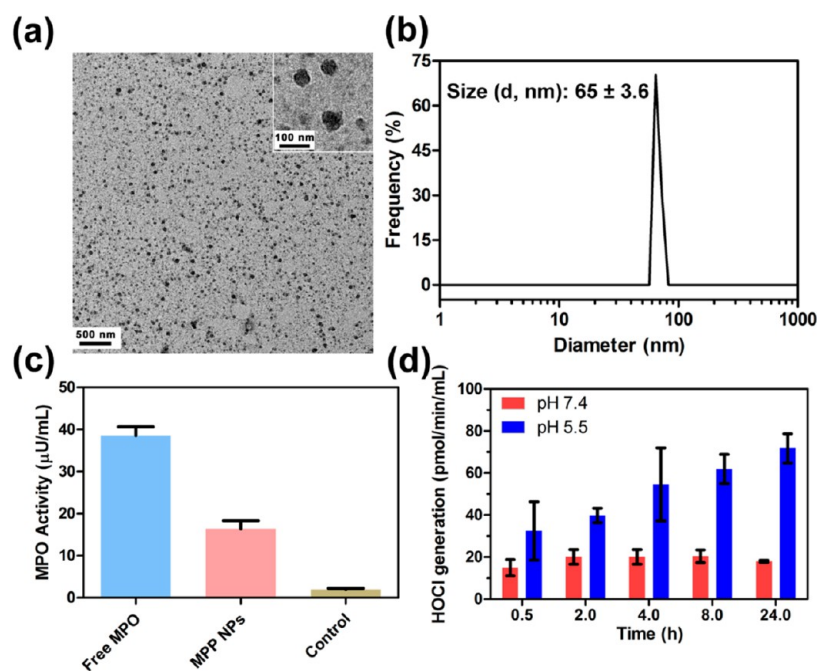


Figure 1. (a) TEM of MPP NPs. (b) DLS of MPP NPs in water. (c) MPO activity from free MPO ($1 \mu\text{g/mL}$), MPP NPs ($1 \mu\text{g/mL}$), and the control group. (d) HOCl generation from the MPP NPs (MPO, $1 \mu\text{g/mL}$) under various pH conditions.

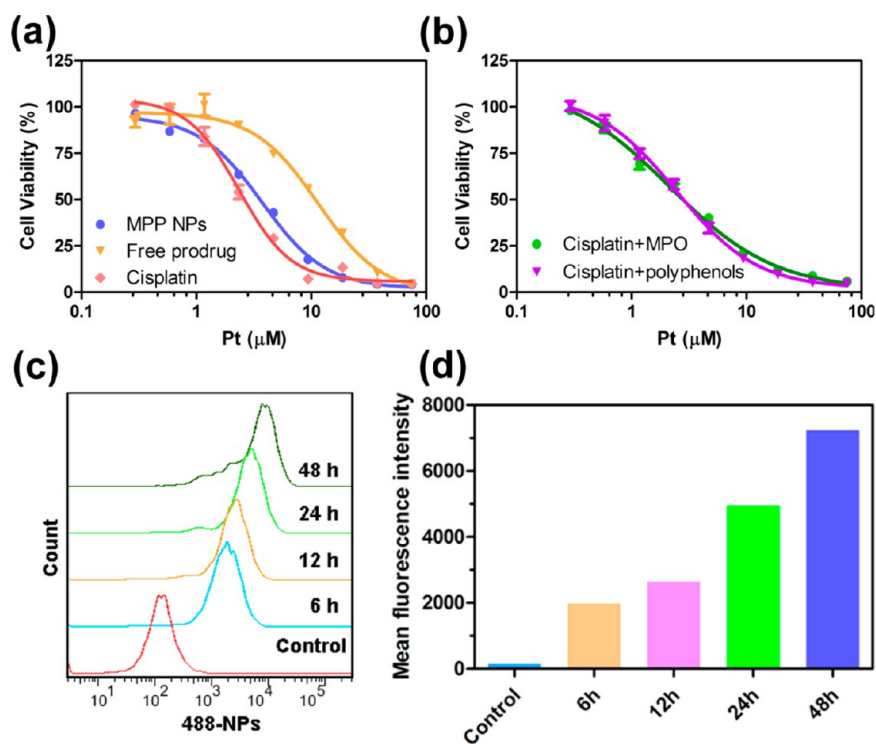


Figure 2. U87MG cell viability profiles of (a) MPP NPs, free cisplatin, free prodrug, and (b) cisplatin plus MPO, cisplatin plus polyphenols for 48 h. (c) Cell uptake of AF488-labeled MPP NPs after 6, 12, 24, and 48 h incubation by flow cytometry. (d) Mean fluorescence intensity of cells after various incubation times.

spectroscopy (EDX) and ICP-OES were used to identify the components of MPP NPs. The peak of Fe and Pt can be clearly seen from EDX (Figure S4). In addition, the signal of Si was from the silicon chip substrates, and Cl was from both PBS buffer and Pt prodrug polyphenols. The components of MPP NPs are given in Table S1, and the PEG polyphenols were the main components, which prolong the blood circulation and reduce

the interaction with blood proteins. Furthermore, the platinum prodrug polyphenols were also as high as 23 wt %, which strongly improved the therapeutic efficacy. The MPO contributed about 2% of the total MPP NPs, the amount of which is sufficient to achieve prodigious HOCl generation from H_2O_2 . The transmission electron microscopy (TEM) image clearly revealed the monodisperse spherical MPP NPs (Figure 1a). The mean

hydrodynamic diameter of MPP NPs measured by dynamic light scattering (DLS) was 65 ± 3.6 nm with a polydispersity index (PDI) of 0.206 (Figure 1b), which matched well with the TEM result. Without the addition of MPO at the beginning, only polydispersed coordination complex aggregates were obtained (Figure S5). Conversely, when 150 kDa MPO protein was employed as the nanotemplate, the subsequent formation of coordination networks resulted in the production of distinct particles.

In Vitro Cell Cytotoxicity, Cell Association, ROS Generation, and Penetration of MPP NPs. First, the activity of MPO was investigated by an MPO assay kit (BioVision's MPO activity fluorometric assay kit). The mechanism features the production of HOCl by MPO catalysis from H_2O_2 , which can react with aminophenyl fluorescein (APF) to generate fluorescein stoichiometrically with dose-dependent fluorescence. Importantly, hypochlorite ion can be selectively detected by APF to differentiate from the other hydroxyl radicals. The MPO activity from the MPP NPs was measured following the kit protocol. The coating of MPNs on the surface of MPO did not significantly influence the activity of MPO. The activity of MPP NPs was still as high as 16.3 ± 1.92 μ U/mL (Figure 1c) in the tube. In addition, the activity of MPO in both PBS and fetal bovine serum (FBS) was measured over time. As given in Figure S6, the MPO activity in FBS was comparable to that in the PBS group at all time points. The MPO activity only dropped slightly after 24 h of incubation. Furthermore, Pt release at two pH conditions (7.4 and 5.5) was tested to mimic physiological and intracellular lysosomal environments, respectively. As given in Figure S7, the Pt release was pH dependent. When the pH was 5.5, more than 60% of drugs was released. In contrast, the MPP NPs were stable at pH 7.4. The above phenomenon can be attributed to the dissociation of the metal–polyphenols under acidic pH, which matched well with a previous report.²⁹ The HOCl generation of MPP NPs was investigated by monitoring the activity of MPO enzyme under two pH conditions. The HOCl generation can be produced faster under acidic conditions (Figure 1d). There are two factors that affect the HOCl generation. On one hand, the acidic conditions can enhance the activity of MPO.³⁰ On the other hand, the MPP NPs can disassemble and be removed from the surface of MPO, restoring MPO activity. Therefore, the activity of MPO can be shielded in the blood by MPP NPs. Moreover, the Pt drugs release in the cancer cell lysosomal environment and the recovery of MPO generates HOCl at the same time.

The cytotoxic effect of the MPP NPs was initially evaluated by the MTT assay (Figure 2a). U87MG cells were exposed to MPP NPs with various Pt concentrations from 0.3 to 75 μ M for 48 h. Free cisplatin and platinum prodrug polyphenols were used as controls. There was a significant dose-dependent cytotoxicity for all three groups. The IC_{50} of MPP NPs was 3.72 μ M, which was comparable to that of cisplatin ($IC_{50} = 2.36$ μ M). As cisplatin is a small-molecule anticancer drug, it can diffuse into cancer cells quickly *in vitro*. The MPP NPs need to enter cancer cells by endocytosis, which is energy-dependent and relatively slow. Moreover, the toxicity of MPP NPs was higher than free platinum prodrug *in vitro*. Compared with the platinum prodrug polyphenols ($IC_{50} = 11.5$ μ M), the MPP NPs exhibited a robust enhancement of cytotoxicity thanks to the ROS generation by MPP NPs. The U87MG cell viability of cisplatin plus MPO and cisplatin plus polyphenols has also been evaluated as the negative control (Figure 2b). 5-Hydroxydopamine hydrochloride (HDA) was used as the polyphenols for the combination cytotoxicity

study with cisplatin because HDA was the reactant of the platinum prodrug polyphenols. The molar ratio between HDA and cisplatin was 2:1, which matched the molar ratio of polyphenols and platinum in the platinum prodrug polyphenols. The molar ratio between MPO and Pt was 1:200. The IC_{50} values of cisplatin plus MPO and cisplatin plus polyphenols were 2.15 and 2.46 μ M, respectively. The above results were similar to free cisplatin ($IC_{50} = 2.36$ μ M). Neither MPO nor polyphenols affected the toxicity of cisplatin significantly. That may be attributed to the low concentration and low toxicity of polyphenols and MPO.

The cell association of MPP NPs was investigated by flow cytometry (Figure 2c and d) and confocal microscopy (Figure S8). The MPP NPs were labeled with AF488 by conjugating the PEG polyphenols and AF488 cadaverine. The AF488-labeled MPP NPs were incubated with U87MG cells for 6, 12, 24, and 48 h at 2 μ M Pt. A longer incubation time resulted in a higher cell association. The mean fluorescence intensity increased from 1979 to 7238 as the incubation time progressed from 6 to 24 h. In addition, the cell uptake of AF488-labeled MPP NPs was investigated by confocal microscopy. As given in Figure S8, more MPP NPs were internalized as the incubation time increased from 2 to 12 h, which was consistent with the flow cytometry results. A flow cytometry cell apoptosis study was further performed to evaluate the cytotoxicity mechanism by the annexin V Alexa Fluor 488 (AF488) and propidium iodide (PI) kit. As given in Figure 3, the U87MG cells treated with MPP NPs

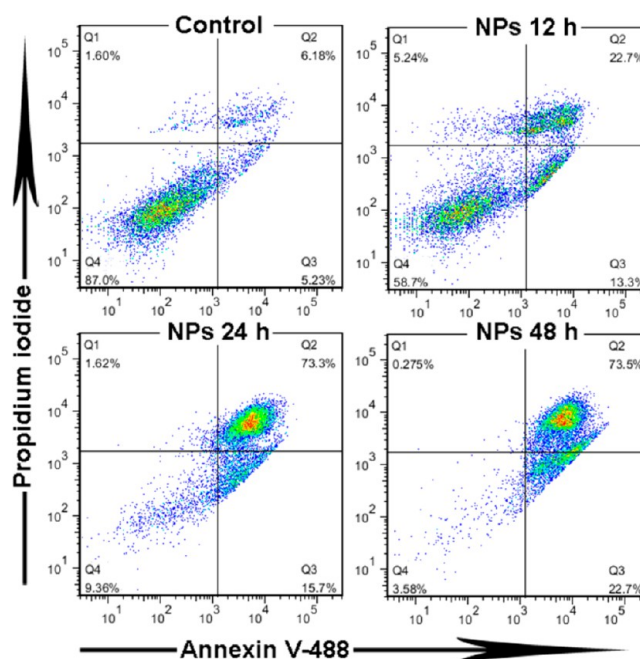


Figure 3. Cell apoptosis of U87MG cells after treatment with MPP NPs for 12, 24, and 48 h.

induced significant time-dependent apoptosis enhancement. The percentage of apoptotic indices increased sharply from 36% (12 h) to 96.2% (48 h).

The internalized platinum drug can promote H_2O_2 generation, which can be catalyzed to HOCl and $O_2^{\cdot-}$ by MPO and ferric ion, respectively. The $O_2^{\cdot-}$ ROS generation by MPP NPs was further confirmed by 2',7'-dichlorodihydrofluorescein diacetate (H_2DCFDA), which can be converted by ROS to highly fluorescent 2',7'-dichlorofluorescein (DCF).³¹ Chlorin e6

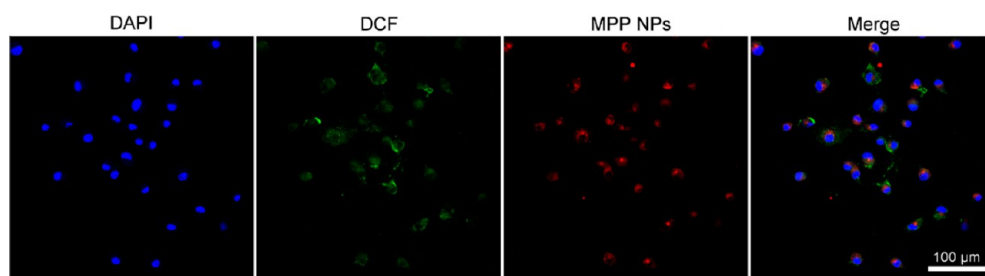


Figure 4. Confocal microscopy images of U87MG cells incubated with MPP NPs for 8 h. The nucleus is stained with DAPI, and the green and red correspond to the DCF of the ROS probe and the Ce6-labeled MPP NPs, respectively.

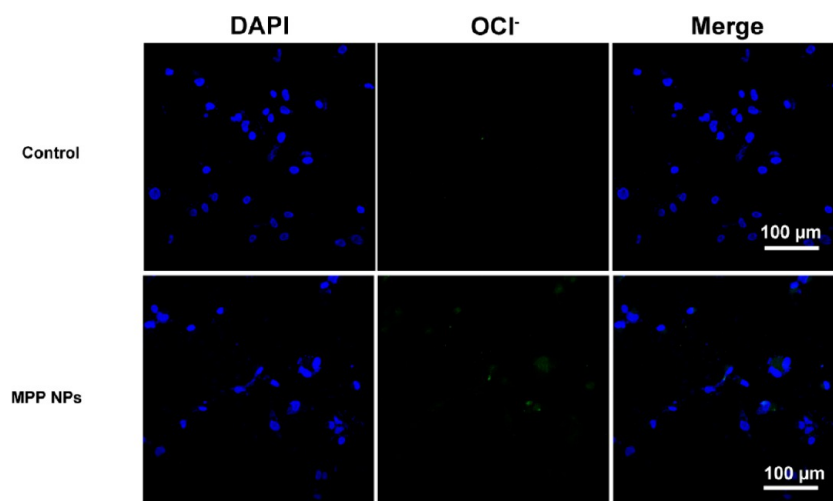


Figure 5. Confocal microscopy images of the OCI⁻ generation from U87MG cells after incubation with MPP NPs for 8 h.

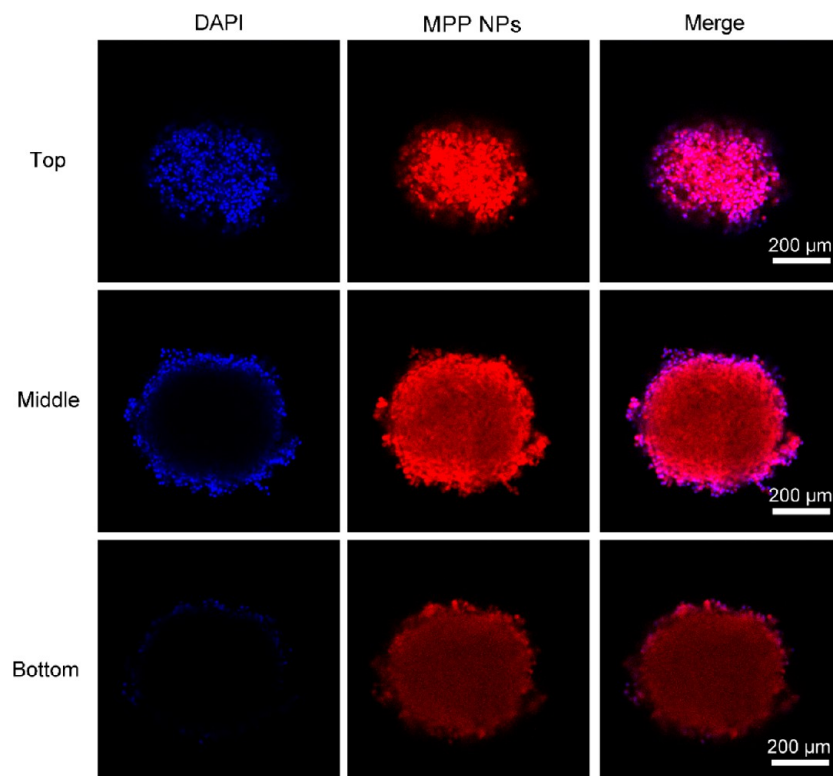


Figure 6. Representative images of the U87MG cell spheroid incubated with Ce6-labeled MPP NPs for 24 h from the top, middle, and bottom regions. The nucleus is stained with DAPI, and the red corresponds to the Ce6-labeled MPP NPs.

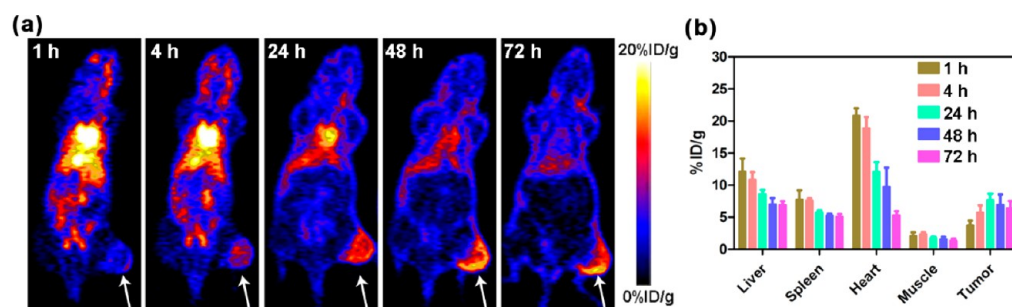


Figure 7. (a) Whole-body PET images of U87MG xenograft tumor mice 1, 4, 24, 48, and 72 h after intravenous injection of ^{89}Zr MPP NPs. The arrows indicate the tumor location. (b) Quantitative region of interest (ROI) analysis of liver, spleen, heart, muscle, and tumor at 1, 4, 24, 48, and 72 h postinjection by PET.

(Ce6)-labeled MPP NPs were incubated with U87MG cells for 8 h and further incubated with H_2DCFDA for 20 min. A large amount of ROS was detected from the cells (Figures 4 and S9 with high magnification). The red fluorescence originated from the Ce6-labeled MPP NPs located in the intracellular compartment of the cytoplasm. The images revealed that the MPP NPs were internalized by U87MG cells and led to greater $\text{O}_2^{\bullet-}$ ROS generation. Moreover, to evaluate intracellular generation of OCI^- from MPP NPs, several control groups (cisplatin, prodrugs, cisplatin + Fe^{3+} , MPO + H_2O_2) have been investigated by APF probe, which can detect OCI^- selectively from the other hydroxyl radicals. As given in Figures 5 and S10, the strong green fluorescence can be observed in the U87MG cells from the MPP NPs group due to the OCI^- generation by a cascade of bioreactions and MPO catalysis. Combined with the other control groups, the MPO and H_2O_2 (50 μM) combination can also generate OCI^- because the H_2O_2 can be catalyzed by free MPO to generate OCI^- .

As we know, the restricted interstitial transport in dense solid tumor limits nanoparticles and therapeutic efficacy. To evaluate the penetration behavior of MPP NPs in an *in vitro* tumor model, a multicellular spheroid (MCS) model based on U87MG cells was chosen. As shown in Figure 6, the MCS has a spherical shape with a diameter of $\sim 500 \mu\text{m}$. After incubating the Ce6-labeled MPP NPs with MCS for 24 h, the MCS was imaged from the top to bottom by Z-stack collection and Z-projection (Figures S11 and S12). Representative images were selected from three regions (top, middle, and bottom). Due to the limited penetration of blue light, the DAPI channel can be observed only on the periphery of the MCS. The Z stack MPP NPs' fluorescence intensity of each image is also given in Figure S13. Interestingly, the MPP NPs' fluorescence was observed not only on the surface but also throughout the whole spheroid. The above results indicated that the MPP NPs exhibited excellent tumor penetration. In addition, the commercial polystyrene (PS) fluorescent particles (Nile red labeled PS particles) with diameters of 100–300 nm were used as a control group. As given in Figure S14, the size of MCS was around 500 μm , and the PS particles were incubated with MCS for 24 h. Three representative images were chosen from the top, middle, and bottom regions. The PS particles were located only on the surface of the MCS and would not be able to penetrate to the core of MCS. There are two reasons to explain the above phenomenon. On one hand, the size of MPP NPs ($\sim 65 \text{ nm}$) is essential for the penetration. The MCS has a dense structure; only small sized particles can achieve deep penetration.³² On the other hand, the high ratio of PEG in the MPP NPs not only prolongs blood circulation but also improves tumor penetration.

Nance *et al.* reported that PEG-modified poly(lactic-co-glycolic acid) (PLGA) nanoparticles showed 100-fold faster penetration than similarly sized PLGA particles without PEG modification.³³ PEGylation of nanoparticles can avoid the interactions between NPs and the tumor extracellular matrix.

In Vivo PET Imaging, Biodistribution, and Cancer Therapy. After validating the good tumor penetration behavior of MPP NPs, positron emission tomography (PET) was employed to investigate the MPP NPs' biodistribution and tumor accumulation.³⁴ In this study, MPP NPs were labeled with ^{89}Zr by conjugating the *p*-isothiocyanatobenzyl-desferrioxamine (DFO) with 8-arm PEG amine with a ratio of 1:8. Then the 8-arm PEG-DFO was further modified with polyphenols. Compared with other isotopes for PET imaging, ^{89}Zr has a relatively long decay half-life (78.4 h).³⁵ As given in Figure 7a, the tumor accumulation of MPP NPs was 3.7%ID/g at 1 h postinjection, which increased to 7.7%ID/g at 24 h. At 72 h, 6.4%ID/g retained in the tumor. The tumor accumulation of MPP NPs reached a peak after 24 h and dropped slightly after 48 and 72 h postinjection. The accumulation of Pt in the tumor was also measured by ICP-OES. As given in Figure S15, the tumor accumulation of Pt increased from 3.3%ID/g at 1 h postinjection to 7.4%ID/g at 24 h. At 72 h postinjection, the tumor accumulation of Pt was still as high as 4.6%ID/g tumor. The ICP results were consistent with PET results. The biodistribution of MPP NPs in the liver, spleen, heart, muscle, and tumor at various postinjection time points is given in Figure 7b. It was found that the MPP NPs in liver had comparable accumulation with that in the tumor due to the high PEG ratio ($>70\%$ by mass) in MPP NPs, which can reduce the uptake by the mononucleosis phagocytosis system. Interestingly, the MPP NPs in the heart were higher than in other organs at 24 h postinjection owing to the heart containing a certain amount of blood and excellent retention performance of MPP NPs in blood. The gamma counter was further used to measure the radioactivity in all the major organs at 72 h postinjection (Figure S16), suggesting the high accumulation of MPP NPs in tumor and deposition of MPP NPs in the liver and spleen. Due to the high heart accumulation of MPP NPs, long-term cardiac toxicity was evaluated by H&E staining. MPP NPs were injected into nude mice with a Pt dose of 2 mg/kg three times. After 6 weeks, the H&E staining images were recorded from the MPP NPs group and PBS group. Compared with the PBS group (Figure S17a and c), there was no evidence of structural cardiac damage or heart muscle damage in the MPP NPs group (Figure S17b and d), indicating no discernible cardiac toxicity of MPP NPs. The above results made sense because the percentage of MPP in MPP NPs was not high

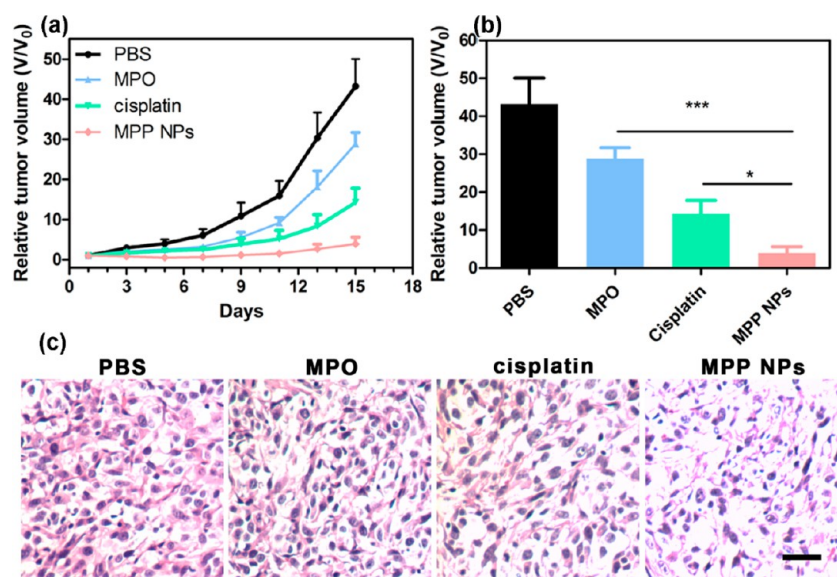


Figure 8. (a) Tumor growth curve of U87MG xenograft tumor mice after various treatments. (b) Relative tumor volume on the 15th day. * $P < 0.05$, ** $P < 0.01$, *** $P < 0.001$. (c) Images of H&E-stained tumor sections from the U87MG tumor bearing mice treated with PBS, MPO, cisplatin, and MPP NPs; the scale bar is 20 μm .

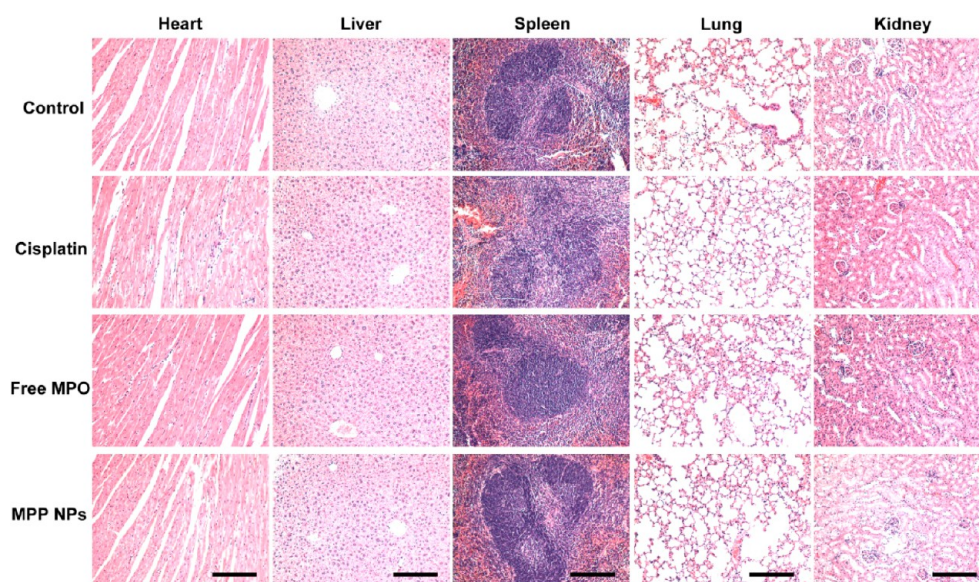


Figure 9. Hematoxylin and eosin (H&E) staining of the major organs (heart, liver, spleen, lung, and kidney) from various groups on the 15th day of treatment. The scale bars are 100 μm .

and the MPP NPs circulated in the blood and accumulated in the tumor.

In vivo antitumor inhibition studies were further performed by a U87MG xenograft tumor model in nude mice. There were four treatment groups: MPP NPs (dose of Pt at 1 mg/kg), cisplatin (dose of Pt at 1 mg/kg), free MPO (20 $\mu\text{g}/\text{kg}$), and PBS by *i.v.* injection on days 1, 3, and 5. As given in Figure 8a,b and Figure S18, treatment with MPP NPs expressed significantly higher antitumor activity compared with free cisplatin at the same dose. There was no significant difference between the MPO and PBS groups, possibly because low MPO can accumulate in the tumor due to the small MW and the fact that most MPO can be readily eliminated from the bloodstream. Additionally, another three formulas of prodrugs (dose of Pt at 1 mg/kg), cisplatin plus MPO (dose of Pt at 1 mg/kg and dose of MPO at 20 $\mu\text{g}/\text{kg}$), and cisplatin plus HDA (dose of Pt at 1 mg/kg and dose of HDA at

2.1 mg/kg) were used as negative control groups. As given in Figure S19, the cisplatin plus MPO and cisplatin plus polyphenols exhibited similar tumor inhibition to cisplatin, and the tumor inhibition effect of the Pt prodrug was lower than that of cisplatin. The above results could be attributed to the low accumulation by small molecules of cisplatin, MPO, HDA, and prodrug. The mice treated with MPP NPs exhibited a much longer survival time (Figure S20). Moreover, the hematoxylin and eosin (H&E) staining of tumor sections from MPP NPs showed the most significant tumor cell apoptosis and necrosis compared with the other control groups (Figure 8c). These results confirmed the effective tumor growth inhibition of MPP NPs. Furthermore, no significant body weight change was observed during all the treatments (Figure S21). Moreover, the histological analysis of major organs (heart, liver, spleen, lung, and kidneys) showed that there were no noticeable histological

changes (Figure 9). All these results indicated that the MPP NPs had good biocompatibility and did not induce discernible side effects *in vivo*.

CONCLUSIONS

We have successfully demonstrated a HOCl-promoted platinum drug therapeutic nanomedicine platform, which encapsulates MPO within the platinum prodrug polyphenols and PEG polyphenols network with ferric ion as the cross-linker. The platinum prodrug loading efficiency was as high as 23%. The MPP NPs can generate highly toxic HOCl by a three-step cascade bioreaction. Owing to the high PEG ratio (>70% by mass) in the MPP NPs, the MPP NPs showed prolonged blood circulation. Therefore, the tumor accumulation is up to 7.7%ID/g as quantified by PET imaging. The MPP NPs showed more effective cancer treatment *in vivo* in suppressing tumor growth and prolonging survival. This work demonstrates the ability of *in situ* HOCl generation by MPO for cancer treatment. Moreover, the MPO encapsulation process by MPNs can be expanded to different enzymes, polyphenol derivatives, and metals, suggesting that this promising strategy could address challenges in related bioapplications.

EXPERIMENTAL SECTION

Synthesis of the Pt(IV) Prodrug Polyphenols. *c,c,t*-Pt-(NH₃)₂Cl₂(O₂CCH₂CH₂COOH)₂ was prepared by a modified literature procedure.³⁶ Then, the Pt(IV) prodrug polyphenols were synthesized by the previous method.²⁸ The *c,c,t*-Pt-(NH₃)₂Cl₂(O₂CCH₂CH₂COOH)₂ (107 mg), DCC (82 mg), and NHS (34 mg) were added in dimethylformamide (DMF) and degassed by nitrogen for 1 h. After that, 5-hydroxydopamine hydrochloride (205 mg) and triethylamine (TEA) (134 μL) were added in the mixture for 24 h. Dichloromethane was added in the system for precipitation. The precipitate was collected by centrifugation (4000 rcf, 10 min). Water was used to dissolve the pellet; then the aqueous solution was run by HPLC to gain the final product Pt(IV) prodrug polyphenols.

Synthesis of PEG Polyphenols. The PEG polyphenols were prepared following a previously published method.²⁹ Eight-arm-PEG-NHS (20 kDa, 100 mg) and dopamine hydrochloride (38 mg) were mixed with DMF (5 mL) under argon bubbling for 1 h. Then TEA (34 μL) was mixed into the above solution under argon protection overnight. To obtain the PEG polyphenols, the reaction mixture was purified by dialysis for 2 days, followed by lyophilization.

Preparation of MPP NPs. The myeloperoxidase (MPO, 10 μL, 100 μg mL⁻¹ in PBS) was added in water (40 μL). Then the Pt(IV) prodrug polyphenols (15 mg mL⁻¹, 5 μL), PEG polyphenols (150 mg mL⁻¹, 5 μL), and FeCl₃ (3 mg mL⁻¹, 5 μL) were added to the solution and mixed for 30 s. Finally, Tris buffer was added in the solution to adjust the pH to 7.6. The resulting MPP NPs were washed by centrifugal filters (30 k) twice. The concentrations of platinum were detected by ICP-OES.

Pt Release from the MPP NPs. The Pt release was recorded by a dialysis process. The MPP NPs (0.5 mL, 5 mg/mL) were dispersed at two PBS solutions (pH 7.4 and 5.5) and injected into the presoaked dialysis cassettes, which were dialyzed against 10 mL PBS solutions (pH 7.4 and 5.5). The release of Pt from the dialysate was measured by ICP-OES under predetermined times.

⁸⁹Zr Radiolabeling Processing. The 8-arm PEG polyphenols with DFO were incubated with ⁸⁹Zr-oxalate at 37 °C for 30 min. Then the above solution was mixed with MPO (10 μL, 100 μg mL⁻¹ in PBS), Pt(IV) prodrug polyphenols (15 mg mL⁻¹, 5 μL), PEG polyphenols (150 mg mL⁻¹, 5 μL), and FeCl₃ (3 mg mL⁻¹, 5 μL). The resulting ⁸⁹Zr-MPP NPs were washed by PBS (300 μL each time) with Amicon Ultra centrifugal filters (0.5 mL, 30 K MWCO) twice.

Three-Dimensional Multicellular Spheroid Model (U87MG Cells). Corning spheroid microplates were employed to construct the multicellular spheroid model. Briefly, U87MG cells were cultured for 6 days to have multicellular spheroids. The cultured medium was replaced

by fresh medium with Ce6-labeled MPO@Pt NPs (1 μM Pt) or Nile red labeled PS particles (10⁻³ % w/v) for another 24 h. Furthermore, the multicellular spheroids were washed by PBS twice and stained by mounting medium with DAPI for 6 h. Finally, all the multicellular spheroids were measured by a confocal microscope (Zeiss LSM 780) with a 10× objective.

Animal Experiments. All procedures were conducted in accordance with and approved by the National Institutes of Health Clinical Center Animal Care and Use Committee (NIH CC/ACUC). Female nude mice were inoculated with U87MG cells (4 × 10⁶) on the flank of each mouse. The U87MG-tumor-bearing mice were randomized into four groups. When the tumor volume was around 80 mm³, the *in vivo* treatment studies were started. The mice were injected with MPP NPs (1 mg/kg Pt), cisplatin (1 mg/kg Pt), free MPO (20 μg/kg), and PBS every other day, three times. For the cisplatin negative control groups, the mice were injected with cisplatin plus HDA (1 mg/kg Pt, 2.1 mg/kg HDA), cisplatin plus MPO (1 mg/kg Pt, 20 μg/kg MPO), and Pt prodrug polyphenols (1 mg/kg Pt) every other day, three times. The tumor size and body weight were monitored every other day. The tumor volume was calculated using the formula $LW^2/2$, where *L* and *W* refer to the length and width of the tumor. To investigate the accumulation of Pt in tumor, the MPP NPs were injected into U87MG-tumor-bearing mice with a Pt dose of 1.5 mg/kg by tail vein when the tumor size reached ~500 mm³. Then the mice were euthanized at 1, 4, 24, 48, and 72 h after injection (three mice per time point). All the tumors were excised and dissolved in nitric acid at 50 °C. The accumulation of Pt in the tumor was measured by ICP.

ASSOCIATED CONTENT

Supporting Information

The Supporting Information is available free of charge on the ACS Publications website at DOI: 10.1021/acsnano.7b06852.

Chemicals, materials, and general characterization; cell experiment, ¹H NMR spectra of *c,c,t*-Pt-(NH₃)₂Cl₂(O₂CCH₂CH₂COOH)₂, platinum prodrug polyphenols and PEG polyphenols; MPO activity in tubes, confocal microscopy images of MPP NPs cell uptake, and U87MG cell spheroid; biodistribution of MPP NPs in different organs, mice survival rate, and body weight curves (PDF)

AUTHOR INFORMATION

Corresponding Authors

*E-mail: wangzl@xidian.edu.cn.

*E-mail: shawn.chen@nih.gov.

ORCID

Yunlu Dai: 0000-0003-4023-7320

Zhen Yang: 0000-0003-4056-0347

Xiaoyuan Chen: 0000-0002-9622-0870

Notes

The authors declare no competing financial interest.

ACKNOWLEDGMENTS

This study was supported by National Key Research and Development Program of China (Nos. 2017YFA0205200 and 2017YFC1309100), National Natural Science Foundation of China (Nos. 81671753 and 81227901), the National 1000 Young Talents Program of China, and the Intramural Research Program of the National Institute of Biomedical Imaging and Bioengineering (NIBIB), National Institutes of Health. We thank Dr. Yijing Liu (NIBIB) for the EDX experiment, we acknowledge Maryland NanoCenter and its NispLab. NispLab is supported, in part, by the NSF in partnership with MRSEC Shared Experimental Facilities.

REFERENCES

- (1) Sabharwal, S. S.; Schumacker, P. T. Mitochondrial ROS in cancer: initiators, amplifiers or an Achilles' heel? *Nat. Rev. Cancer* **2014**, *14*, 709–721.
- (2) Trachootham, D.; Alexandre, J.; Huang, P. Targeting cancer cells by ROS-mediated mechanisms: a radical therapeutic approach? *Nat. Rev. Drug Discovery* **2009**, *8*, 579–591.
- (3) Rodriguez, R.; Redman, R. Balancing the generation and elimination of reactive oxygen species. *Proc. Natl. Acad. Sci. U. S. A.* **2005**, *102*, 3175–3176.
- (4) Zhou, Z.; Song, J.; Nie, L.; Chen, X. Reactive oxygen species generating systems meeting challenges of photodynamic cancer therapy. *Chem. Soc. Rev.* **2016**, *45*, 6597–6626.
- (5) Fan, W.; Huang, P.; Chen, X. Overcoming the Achilles' heel of photodynamic therapy. *Chem. Soc. Rev.* **2016**, *45*, 6488–6519.
- (6) Wang, D.; Wang, T.; Liu, J.; Yu, H.; Jiao, S.; Feng, B.; Zhou, F.; Fu, Y.; Yin, Q.; Zhang, P.; Zhang, Z.; Zhou, Z.; Li, Y. Acid-Activatable Versatile Micelleplexes for PD-L1 Blockade-Enhanced Cancer Photodynamic Immunotherapy. *Nano Lett.* **2016**, *16*, 5503–5513.
- (7) Chen, Q.; Xu, L.; Liang, C.; Wang, C.; Peng, R.; Liu, Z. Photothermal therapy with immune-adjutant nanoparticles together with checkpoint blockade for effective cancer immunotherapy. *Nat. Commun.* **2016**, *7*, 13193.
- (8) Liang, X.; Li, X.; Yue, X.; Dai, Z. Conjugation of Porphyrin to Nanohybrid Cerasomes for Photodynamic Diagnosis and Therapy of Cancer. *Angew. Chem., Int. Ed.* **2011**, *50*, 11622–11627.
- (9) Zhu, H.; Fang, Y.; Miao, Q.; Qi, X.; Ding, D.; Chen, P.; Pu, K. Regulating Near-Infrared Photodynamic Properties of Semiconducting Polymer Nanotheranostics for Optimized Cancer Therapy. *ACS Nano* **2017**, *11*, 8998–9009.
- (10) Lu, Y.; Aimeetti, A. A.; Langer, R.; Gu, Z. Bioresponsive materials. *Nat. Rev. Mater.* **2016**, *2*, 16075.
- (11) Lucky, S. S.; Soo, K. C.; Zhang, Y. Nanoparticles in Photodynamic Therapy. *Chem. Rev.* **2015**, *115*, 1990–2042.
- (12) Ethirajan, M.; Chen, Y.; Joshi, P.; Pandey, R. K. The role of porphyrin chemistry in tumor imaging and photodynamic therapy. *Chem. Soc. Rev.* **2011**, *40*, 340–362.
- (13) Bánfi, B.; Malgrange, B.; Knisz, J.; Steger, K.; Dubois-Dauphin, M.; Krause, K.-H. NOX3, a Superoxide-generating NADPH Oxidase of the Inner Ear. *J. Biol. Chem.* **2004**, *279*, 46065–46072.
- (14) Singh, D. K.; Winocour, P.; Farrington, K. Oxidative stress in early diabetic nephropathy: fueling the fire. *Nat. Rev. Endocrinol.* **2011**, *7*, 176–184.
- (15) Wilson, J. J.; Lippard, S. J. Synthetic Methods for the Preparation of Platinum Anticancer Complexes. *Chem. Rev.* **2014**, *114*, 4470–4495.
- (16) Liu, D.; Poon, C.; Lu, K.; He, C.; Lin, W. Self-assembled nanoscale coordination polymers with trigger release properties for effective anticancer therapy. *Nat. Commun.* **2014**, *5*, 4182.
- (17) Browning, R. J.; Reardon, P. J. T.; Parhizkar, M.; Pedley, R. B.; Edirisinghe, M.; Knowles, J. C.; Stride, E. Drug Delivery Strategies for Platinum-Based Chemotherapy. *ACS Nano* **2017**, *11*, 8560–8578.
- (18) Ma, P. a.; Xiao, H.; Yu, C.; Liu, J.; Cheng, Z.; Song, H.; Zhang, X.; Li, C.; Wang, J.; Gu, Z.; Lin, J. Enhanced Cisplatin Chemotherapy by Iron Oxide Nanocarrier-Mediated Generation of Highly Toxic Reactive Oxygen Species. *Nano Lett.* **2017**, *17*, 928–937.
- (19) Huang, G.; Chen, H.; Dong, Y.; Luo, X.; Yu, H.; Moore, Z.; Bey, E. A.; Boothman, D. A.; Gao, J. Superparamagnetic iron oxide nanoparticles: amplifying ROS stress to improve anticancer drug efficacy. *Theranostics* **2013**, *3*, 116–126.
- (20) Nimse, S. B.; Pal, D. Free radicals, natural antioxidants, and their reaction mechanisms. *RSC Adv.* **2015**, *5*, 27986–28006.
- (21) Zheng, D.-W.; Lei, Q.; Zhu, J.-Y.; Fan, J.-X.; Li, C.-X.; Li, C.; Xu, Z.; Cheng, S.-X.; Zhang, X.-Z. Switching Apoptosis to Ferroptosis: Metal–Organic Network for High-Efficiency Anticancer Therapy. *Nano Lett.* **2017**, *17*, 284–291.
- (22) Nakazato, T.; Sagawa, M.; Yamato, K.; Xian, M.; Yamamoto, T.; Suematsu, M.; Ikeda, Y.; Kizaki, M. Myeloperoxidase Is a Key Regulator of Oxidative Stress–Mediated Apoptosis in Myeloid Leukemic Cells. *Clin. Cancer Res.* **2007**, *13*, 5436–5445.
- (23) Gaut, J. P.; Yeh, G. C.; Tran, H. D.; Byun, J.; Henderson, J. P.; Richter, G. M.; Brennan, M.-L.; Lulis, A. J.; Belaouaj, A.; Hotchkiss, R. S. Neutrophils employ the myeloperoxidase system to generate antimicrobial brominating and chlorinating oxidants during sepsis. *Proc. Natl. Acad. Sci. U. S. A.* **2001**, *98*, 11961–11966.
- (24) Zhang, X. Y.; Elfarra, A. A. Potential roles of myeloperoxidase and hypochlorous acid in metabolism and toxicity of alkene hydrocarbons and drug molecules containing olefinic moieties. *Expert Opin. Drug Metab. Toxicol.* **2017**, *13*, 513–524.
- (25) Lloyd, M. M.; van Reyk, D. M.; Davies, M. J.; Hawkins, C. L. Hypothiocyanous acid is a more potent inducer of apoptosis and protein thiol depletion in murine macrophage cells than hypochlorous acid or hypobromous acid. *Biochem. J.* **2008**, *414*, 271–280.
- (26) Ejima, H.; Richardson, J. J.; Liang, K.; Best, J. P.; van Koeverden, M. P.; Such, G. K.; Cui, J.; Caruso, F. One-Step Assembly of Coordination Complexes for Versatile Film and Particle Engineering. *Science* **2013**, *341*, 154–157.
- (27) Guo, J.; Ping, Y.; Ejima, H.; Alt, K.; Meissner, M.; Richardson, J. J.; Yan, Y.; Peter, K.; von Elverfeldt, D.; Hagemeyer, C. E.; Caruso, F. Engineering Multifunctional Capsules through the Assembly of Metal–Phenolic Networks. *Angew. Chem., Int. Ed.* **2014**, *53*, 5546–5551.
- (28) Dai, Y.; Guo, J.; Wang, T.-Y.; Ju, Y.; Mitchell, A. J.; Bonnard, T.; Cui, J.; Richardson, J. J.; Hagemeyer, C. E.; Alt, K.; Caruso, F. Self-Assembled Nanoparticles from Phenolic Derivatives for Cancer Therapy. *Adv. Healthcare Mater.* **2017**, *6*, 1700467.
- (29) Ju, Y.; Cui, J.; Muellner, M.; Suma, T.; Hu, M.; Caruso, F. Engineering Low-Fouling and pH-Degradable Capsules through the Assembly of Metal-Phenolic Networks. *Biomacromolecules* **2015**, *16*, 807–814.
- (30) Vlasova, I. I.; Arnhold, J.; Osipov, A. N.; Panasenko, O. M. pH-dependent regulation of myeloperoxidase activity. *Biochemistry (Moscow)* **2006**, *71*, 667–677.
- (31) Zhou, Z.; Song, J.; Tian, R.; Yang, Z.; Yu, G.; Lin, L.; Zhang, G.; Fan, W.; Zhang, F.; Niu, G.; Nie, L.; Chen, X. Activatable Singlet Oxygen Generation from Lipid Hydroperoxide Nanoparticles for Cancer Therapy. *Angew. Chem., Int. Ed.* **2017**, *56*, 6492–6496.
- (32) Sun, Q.; Ojha, T.; Kiessling, F.; Lammers, T.; Shi, Y. Enhancing Tumor Penetration of Nanomedicines. *Biomacromolecules* **2017**, *18*, 1449–1459.
- (33) Nance, E.; Zhang, C.; Shih, T.-Y.; Xu, Q.; Schuster, B. S.; Hanes, J. Brain-Penetrating Nanoparticles Improve Paclitaxel Efficacy in Malignant Glioma Following Local Administration. *ACS Nano* **2014**, *8*, 10655–10664.
- (34) Sun, X.; Cai, W.; Chen, X. Positron Emission Tomography Imaging Using Radiolabeled Inorganic Nanomaterials. *Acc. Chem. Res.* **2015**, *48*, 286–294.
- (35) Chi, C.; Du, Y.; Ye, J.; Kou, D.; Qiu, J.; Wang, J.; Tian, J.; Chen, X. Intraoperative imaging-guided cancer surgery: from current fluorescence molecular imaging methods to future multi-modality imaging technology. *Theranostics* **2014**, *4*, 1072.
- (36) Dai, Y.; Kang, X.; Yang, D.; Li, X.; Zhang, X.; Li, C.; Hou, Z.; Cheng, Z.; Ma, P. a.; Lin, J. Platinum (IV) Pro-Drug Conjugated NaYF₄:Yb³⁺/Er³⁺ Nanoparticles for Targeted Drug Delivery and Up-Conversion Cell Imaging. *Adv. Healthcare Mater.* **2013**, *2*, S62–S67.